Published in final edited form as:
J Immunol. 2019 November 01; 203(9): 2377–2387. doi:10.4049/jimmunol.1900075.

In vivo function of the lipid raft protein flotillin 1 during CD8+ T cell-mediated host surveillance

Xenia Ficht[1], **Nora Ruef**[2], **Bettina Stolp**[1,3], **Guerric P.B. Samson**[4], **Federica Moalli**[1,5], **Nicolas Page**[6], **Doron Merkler**[6], **Ben J. Nichols**[7], **Alba Diz-Muñoz**[8], **Daniel F. Legler**[4], **Verena Niggli**[9], **Jens V. Stein**[2]

[1]Theodor Kocher Institute, University of Bern, 3012 Bern, Switzerland [2]Department of Oncology, Microbiology and Immunology, University of Fribourg, 1700 Fribourg, Switzerland [3]Department for Infectious Diseases, Integrative Virology, Center for Integrative Infectious Disease Research, University Hospital Heidelberg, Im Neuenheimer Feld 344, 69120 Heidelberg, Germany [4]Biotechnology Institute Thurgau (BITg) at the University of Konstanz, Kreuzlingen, Switzerland [5]Division of Immunology, Transplantation and Infectious Diseases and Experimental Imaging Center, IRCCS San Raffaele Scientific Institute, 20132 Milan, Italy [6]Department of Pathology and Immunology, University of Geneva, 1211 Geneva, Switzerland [7]Medical Research Council Laboratory of Molecular Biology, Cambridge, United Kingdom [8]Cell Biology and Biophysics Unit, European Molecular Biology Laboratory, 69117 Heidelberg, Germany [9]Institute of Pathology, University of Bern, 3008 Bern, Switzerland

Abstract

Flotillin-1 (Flot1) is an evolutionary conserved, ubiquitously expressed lipid raft-associated scaffolding protein. Migration of Flot1-deficient neutrophils is impaired due to a decrease in myosin II-mediated contractility. Flot1 also accumulates in the uropod of polarized T cells, suggesting an analogous role in T cell migration. Here, we analyzed morphology and migration parameters of murine WT and Flot1$^{-/-}$ CD8^{+} T cells using *in vitro* assays and intravital two-photon microscopy of lymphoid and non-lymphoid tissues. Flot1$^{-/-}$ CD8^{+} T cells displayed significant alterations in cell shape and motility parameters *in vivo* but showed comparable homing to lymphoid organs and intact *in vitro* migration to chemokines. Furthermore, their clonal expansion and infiltration into non-lymphoid tissues during primary and secondary antiviral immune responses was comparable to WT CD8^{+} T cells. Taken together, Flot1 plays a detectable but unexpectedly minor role for CD8^{+} T cell behavior under physiological conditions.

Address correspondence: Jens V. Stein, Ph. D., Department of Oncology, Microbiology and Immunology, University of Fribourg, Ch. du Musée, 5, 1700 Fribourg, Switzerland, Tel. +41 26 300 8602, jens.stein@unifr.ch.

Author Contributions

XF performed imaging, Atomic force microscopy, transwell, and flow cytometry experiments. NR performed Atomic force microscopy and rechallenge experiments. BS performed chemotaxis and flow cytometry experiments. GPBS performed immunofluorescence and analyzed Flot2$^{-/-}$ cells under supervision of DFL. FM assisted with skin imaging. VN performed western blots and measured pERM capping. NP and DM provided vital material. ADM provided critical assistance for membrane tension measurements. BJN generated the Flot1$^{-/-}$ mouse line. XF and JVS designed experiments and wrote the manuscript with input of all coauthors.

Competing interests

The authors declare no competing interests.

Europe PMC Funders Author Manuscripts

Introduction

Naïve $CD8^+$ T cells (T_N) actively migrate in lymphoid tissue interstitium and use their unique T cell receptor (TCR) to scan dendritic cells (DCs) for cognate peptide presented on major histocompatibility complex-I (pMHC). Upon activation, $CD8^+$ T cells undergo clonal expansion and give rise to cytotoxic effector T cells (T_{EFF}). T_{EFF} spread from lymphoid organs to infected tissue where they kill host cells presenting cognate pMHC in order to eliminate the pool of intracellular pathogens, in particular viruses. After clearance of infections, long-lived memory T cells persist to provide continuous immune surveillance and rapid effector functions in the event of a secondary infection with the same pathogen. Distinct subpopulations of memory $CD8^+$ T cells are categorized according to their functions and tissue homing properties: $CD62L^+$ $CCR7^+$ central memory T cells (T_{CM}) recirculate through lymphoid organs similar to T_N, while $CD62L^-$ $CCR7^-$ effector memory T cells (T_{EM}) recirculate through non-lymphoid organs and blood. In recent years, a novel subset of tissue-resident memory T cells (T_{RM}) were identified. T_{RM} do not recirculate but permanently reside in peripheral organs, including the epidermis and the submandibular salivary gland (SMG). In these organs, T_{RM} mediate rapid recall responses to prevent pathogen spread (1–7).

Studies using intravital twophoton microscopy (2PM) of lymphoid and non-lymphoid organs have uncovered a remarkable motility of T_N, T_{EFF} and memory $CD8^+$ T cells in all tissues analyzed thus far. This behavior is explained by their pMHC restriction, imposing the need to physically interact with DCs and target cells. Thus, the ability of $CD8^+$ T cells to scan their environment through active migration is a key feature maintained throughout all phases of adaptive immune responses. Active movement of T cells requires polarization and constant cytoskeletal rearrangement – most importantly the treadmilling of filamentous actin (F-actin) and its contraction by non-muscle myosin IIa (Myo IIa) (8–12). Thus, isolated T_N cells are round and unpolarized, but rapidly form a polarized amoeboid shape after chemokine stimulation. This shape is characterized by a protrusive leading edge and a contractile cell rear called uropod. Uropod contractility is important for detachment from adhesive substrates and for creating force to squeeze the biggest organelle of a cell, the nucleus, through narrow pores encountered during migration (8, 13, 14). In addition to the Myo IIa activity for actomyosin contraction, the uropod is rich in phosphorylated membrane-to-cytoskeleton-linker proteins of the ezrin/radixin/moesin family (pERM), adhesion receptors such as CD44 and PSGL-1, and cholesterol rich membrane microdomains, the lipid rafts (15). The tip of the uropod of polarized leukocytes also contains flotillin-1 (Flot1; also known as Reggie2) and flotillin-2 (Flot2; Reggie1), evolutionary conserved, ubiquitously expressed membrane-associated scaffolding proteins (16–21). Both flotillins possess N-terminal fatty acid modifications next to or within their prohibitin homology domain (PHB) that target them to lipid rafts (18–21). In leukocytes, C-terminal interactions lead to the hetero-oligomerization of Flot1 and Flot2, which is required for mutual stabilization and targeting to lipid rafts (19, 22). Flotillins have been implicated in a variety of cellular functions, including cell-cell adhesion (19), endocytosis (19), regulation of G-protein coupled receptor signaling (23) and modulation of the actomyosin cytoskeleton of leukocytes. $Flot1^{-/-}$ mice show deficient recruitment of immune cells to

inflammatory sites due to a decreased migratory capacity of neutrophils and monocytes (24). Flot-1$^{-/-}$ neutrophils display reduced levels of phosphorylated myosin regulatory chain, which in turn leads to a defect in Myo IIa activity and cell migration (24). Similarly, Flot1 and Flot2 interdependently cap at uropods of primary human T cells, and expression of a dominant-negative Flot2 mutant or reduced expression of Flot1 impair uropod formation (18, 22, 25). *In vitro* experiments suggest that organization of membrane microdomains by flotillins is required for optimal T cell migration (26). Furthermore, flotillin-containing lipid rafts assemble at immunological synapses (IS) and have been proposed to serve as scaffold for the TCR signaling machinery (27–29). Yet, there is no evidence to date on how Flot1 affects CD8$^+$ T cell-mediated organ surveillance *in vivo*, nor how it impacts T cell activation during adaptive immune responses against microbes.

Here, we analyzed *in vitro* properties and *in vivo* behavior of Flot1$^{-/-}$ CD8$^+$ T cells using functional readouts under physiological conditions in mouse models. Our data suggest that Flot1 is involved in regulating the shape and speed of migrating CD8$^+$ T cells in lymphoid and non-lymphoid tissues, but has only a minor impact on their ability to expand, differentiate and surveille distinct microenvironments. Taken together, our data shed light on the physiological impact of this conserved protein during adaptive immunity mediated by CD8$^+$ T cells.

Materials and Methods

Mice

OT-I TCR transgenic mice (30) were crossed to Tg(UBC-GFP)30Scha “Ubi-GFP” (31) (“GFP$^+$ OT-I”), hCD2-dsRed (32) (“DsRed$^+$ OT-I”) or tdTomato-expressing Ai14 x ZP3 (33, 34) (“tdTom$^+$ OT-I”) mice on the C57BL/6J background. GFP$^+$ OT-I mice were crossed with Flot1$^{-/-}$ mice (24). All mice were bred at the animal facility of the University of Bern and Fribourg, Switzerland, and used as lymphocyte donor mice at 6-20 weeks of age. 6-10 week-old sex-matched C57BL/6J mice (Janvier, France) were used as recipient mice. All experiments were performed in accordance to federal animal experimentation regulations and approved by the cantonal committees.

Reagents

Sodium Pyruvate (100 mM; #11360-039), HEPES buffer (1 M; #15630-056), RPMI 1640 (#21875-034), L-Glutamine (200 mM, #25030-024), Minimum essential Medium Non-essential amino acids (MEM NEAA, #11140-035), and Pen Strep (#15140-122) were purchased from Gibco. Fetal Bovine Serum (FCS, #SV30143.03) was obtained from HyClone.

Cell polarization and pERM capping

Flot1 staining was performed as described (18). Cell polarization and phosphorylated ERM (pERM) capping experiments were performed as described (35). In brief, naïve T cells were isolated from spleen and purified by negative selection. Cells were then incubated for 15 min without or with 200 ng CCL19 at 37°C in suspension followed by fixation with 10% trichloroacetic acid (TCA), staining for pERM (Cell Signaling technologies) and evaluation

Europe PMC Funders Author Manuscripts

of cell morphology and pERM caps. Only cells with pERM staining were evaluated (100 cells counted per sample). For activated T cells, T cells were isolated from spleen and incubated for 2 days with 1 μg/ml ConA, then 4 days with IL-2 (100 Units/ml). Cells were then incubated for 15 min without or with 200 ng CCL19 at 37°C in suspension followed by fixation with 10% TCA, staining for pERM and evaluation of cell morphology and pERM caps. Only cells with pERM staining were evaluated (100 cells counted per sample).

For Flot2 staining, $CD8^+$ T cells were isolated from spleen and LN of $Flot1^{-/-}$ and WT mice using the EasySep™ Mouse $CD8^+$ T cell Isolation Kit (Stem Cell Technologies). Cells were incubated for 4 days with 20 ng/ml IL-7 before use in immunofluorescent staining. Cover glasses were coated with 10 μg/ml fibronectin and 1 μM CCL21. Cells were added and incubated for 1 h at 37°C and fixed with 10% TCA for 5 min at 37°C. Cells were washed twice with PBS, permeabilized with 0.1 mg/ml lysolecithin 10 min at RT and washed again twice with PBS. Cover glasses were blocked with PBS/5% BSA for 1 h and stained o.n. with anti-Flot2 Ab (BD Transduction Laboratories, 1:100 in PBS/0.5% BSA). After washing once with PBS/0.05% Tween-20 and twice with PBS, cells were stained with the secondary antibody goat anti-mouse-AF594 (ThermoFisher, 1:100 in PBS/5% BSA) for 1 h at RT and washed once with PBS/0.05% Tween-20 and twice with PBS. Cover glasses were mounted on a glass slide, let dry o.n. and images were acquired on a Leica TCS SP5 using a 63X glycerol immersion objective (NA 1.3).

Western Blots

Expression of Flot1 and Flot2 was measured in T lymphoblasts isolated from spleens of WT and $Flot1^{-/-}$ mice. To this end, 1.5 x 10^6 T lymphoblasts per sample were precipitated with TCA and separated on 10% sodium dodecyl sulfate polyacrylamide gel electrophoresis (SDS-PAGE) followed by immunoblotting with the specified antibodies (anti-mouse flotillin 1 #610820 and anti-mouse flotillin 2 #610383 from BD Transduction Laboratories). In some experiments, splenocytes from WT or $Flot2^{-/-}$ were lysed with NP-40 lysis buffer [10 mM Tris-HCl (pH 7.6), 150 mM NaCl, 1% NP 40] supplemented with protease inhibitor cocktail (11836170001, Roche). Proteins were resolved by 10% SDS-PAGE, transferred to nitrocellulose blocking membranes (10600002, GE Healthcare) and blocked with 1x Roti-block (A151.4, Roth). Membranes were further incubated with the desired primary antibody solution followed by an HRP-conjugated antibody solution and visualized with clarity western ECL substrate (170-5061, Biorad). Membranes were stripped using Restore Western Blot Stripping Buffer (21063, Thermo Fisher Scientific) for actin staining (loading control).

Transwell migration assays

WT and $Flot1^{-/-}$ OT-I $CD8^+$ T cells (5 x 10^5/well) in 100 μL CM-R (RPMI/10% FCS/1% HEPES/2 mM L-Glutamine/1 mM Na-Pyruvate/PenStrep) were added to the inserts of 3 or 5 μm-pore size Transwell Chambers (Costar) and allowed to migrate towards the indicated concentrations of recombinant CCL21 (Peprotech) for 2 h at 37°C. Percent of transmigrated cells was measured by comparing cell counts of input to Transwells after 1 min of acquisition at the same speed with a FACSCalibur or FACS LSRII flow cytometer (BD).

Membrane tension measurements

CD8$^+$ T cells were isolated with Stem Cell negative selection kit as described above, and kept on ice in CM-R with 5 μg/mL IL-7 (407-ML-005 R&D) until o.n. activation with 2.5 μg/mL ConA. Imaging dishes were washed sonicated for 5 min in water, washed in 99% ethanol, dried, and sterilized with UV-light for 15 min. Dishes were coated for 30-60 min at 37°C with 0.01% Poly-L-Lysine (Sigma Aldrich), and washed 8-10 times with PBS. Approximately 5 x 10^5 T cells were plated onto the coated dish in 0.5 mL CM-R and incubated for 10-15 min at 37°C. Subsequently, dishes were washed carefully 8-10 times with warm medium. For tether measurements, 3 mL CM-R (5% FCS) were added to the dish. Olympus BioLevers (k = 60 pN/nm) were calibrated using the thermal noise method and incubated in 4 mg/ml Concanavalin A (C5275, Sigma) for 1 h at RT. Before the measurements, cantilevers were rinsed in DPBS. Cells were located by brightfield imaging, and the cantilever was positioned at any location over the cell for tether measurement. Cells were not used longer than 1 h for data acquisition. Tethers were pulled using a CellHesion 200 from JPK mounted on an inverted Nikon Ti microscope. Approach velocity was set to 1 μm/s, contact force to 100 – 300 pN, contact time to 5 - 10 s and retraction speed to 10 μm/s. After a 10 μm tether was pulled, the cantilever position was held constant until it broke. Only tethers that broke in less than 15 s were considered, as actin polymerized inside of longer-lived tethers. Negative and positive forces relate to the angle the cantilever takes, but the sign is arbitrary. By convention, contacting the cell deflects the cantilever towards positive values. Conversely, when the cantilever is pulled downwards by a membrane tether, the values are negative. Resulting force–time curves were analyzed with the JPKSPM Data Processing Software.

T cell transfer and infections

Negative isolation of CD8$^+$ T cells from peripheral lymph nodes and spleen of CD45.1$^+$, dsRed$^+$, tdTom$^+$, GFP$^+$ OT-I or Flot1$^{-/-}$ GFP$^+$ OT -I mice was performed using EasySep™ Mouse CD8$^+$ T cell Isolation Kit (Stem Cell Technologies). We confirmed CD8$^+$ T cell purity to be >90% by flow cytometry and transferred 10^4 or 0.5-1 x 10^6 OT-I cells in CM-R i.v. 1 day before LCMV-OVA or HSV-1$_{TOM-OVA}$ infection, respectively. For some experiments, co-transfer of equal amounts of Flot1$^{+/+}$ GFP$^+$ OT-I or Flot1$^{-/-}$ GFP$^+$ OT-I and Flot1$^{+/+}$ dsRed$^+$, CD45.1$^+$ or tdTom$^+$ OT-I was performed. Mice were either i.p. infected with 1 x 10^5 pfu LCMV-OVA (36) or anesthetized, shaved, and tattooed with 5 x 10^5 pfu in 10 μL of HSV-1$_{TOM-OVA}$ using a Cheyenne tattooing machine as described (6). Experimental read-outs for the acute, cleared and memory phase of LCMV infection were performed 6, 15 and > than 28 days p.i., respectively. Experimental read-outs for memory phase of HSV infection were performed later than 28 days p.i. For rechallenge experiments, LCMV-OVA-infected mice in the memory phase (> 30 days p.i.) were bled to assess the ratio of WT and Flot1$^{-/-}$ OT-I T cells as correction factor before receiving 5 x 10^3 cfu OVA-expressing Listeria monocytogenes (Lm) i.v. (37).

Flow cytometry

At indicated time points, spleens and PLN were harvested and organs were passed through cell strainers (70 μm; Bioswisstec) to obtain single cell suspensions. Red blood cell lysis was

performed on splenocytes. SMG was minced and treated with 2 U/μl collagenase II (Worthington Biochem) in CM-R for 45 min at 37°C, passed through a 70 μm cell strainer and washed with PBS/10 mM EDTA. Tattooed skin was minced and digested in 0.25% Trypsin/EDTA (Gibco) for 30 min at 37°C and passed through a cell strainer and washed with PBS/5 mM EDTA. We used the following reagents for flow cytometry: anti-CD4-PE (GK1.5); anti-CD8α-PerCP (53-6.7), anti-CD8α-APC (53-6.7), anti-CD8α-APC/Fire750 (53-6.7; all from BioLegend), anti-CD16/32 (Fc-block; 2.4G2, StemCell), anti-CD44-PE (IM7, BD Biosciences), anti-CD45.1-PE (A20, BioLegend), anti-CD45-PE (30-F11, BD Biosciences), anti-CD45-PerCP (30-F11), anti-CD62L-APC (MEL-14), anti-CD103-Biotin (M290), anti-CD103-APC (2E7; all from Biolegend), anti-CD127-Biotin (B12-1, BD Pharmingen), anti-CD127-APC (A7R34), anti-KLRG1-PECy7 (2F1/KLRG1), anti-KLRG1-PE (2F1/KLRG1), Streptavidin-BV421 and Streptavidin-PE (all from Biolegend). Cell suspensions were stained on ice for 20 min with indicated antibodies and washed in FACS buffer (PBS/2% FCS/1 mM EDTA). For acute phase stainings, cells were fixed for 20 min in 1% PFA after staining. Cells were washed again prior to acquisition and at least 10^5 cells in the FSC/SSC “lymphocyte” gate were acquired using a FACSCalibur or LSR II (BD Bioscience). Total cell counts were measured by acquiring single cell suspensions in PKH26 reference microbeads (Sigma), or Beckman coulter counting beads (REF7547053) for 1 min at high speed or by counting with FastRead counting slides (Immune Systems Ltd). Gating for CD103, CD127 and KLRG1 was set according to isotype or FMO controls. Data was analyzed with FlowJo (FlowJo LLC).

T cell homing

$DsRed^+$ and GFP^+ $Flot1^{-/-}$ $CD8^+$ T cells mice were injected i.v. into sex-matched recipients (2-3 x 10^6 cells/mouse). After 2 h, mice were killed and perfused with PBS. Peripheral LN, mesenteric LN, Peyer’s Patches, and spleen were harvested and passed through passed through a 70 μm cell strainer. Afterwards, erythrocytes in spleen were lysed in RBC buffer for 5 min. Blood was harvested by taking it up directly from the vena cava during perfusion into a 20 ml syringed filled with 10 mL of PBS/10 mM EDTA. Samples were stained on ice with PerCP-conjugated anti-mouse CD8α, washed and acquired on a FACSCalibur flow cytometer (BD). Ratio of $Flot1^{-/-}$ to WT cells in each organ was normalized to input.

Twophoton microscopy (2PM) intravital imaging

2PM intravital imaging of the popliteal LN and skin was performed as previously described (38). In short, ketamine/xylazine/acepromazine was used to anesthetize mice and the right popliteal LN was surgically prepared. For skin imaging, hair on the right flank was removed and a section of skin was elevated onto a metal holder by making two parallel incisions. Prior to imaging, Alexa 633-conjugated MECA-79 (10 μg/mouse) was injected i.v. to mark HEV in LN. 2PM imaging was carried out with a TrimScope I 2PM microscope using a 25X Nikon (NA 1.0) or 20X Olympus (NA 0.95) objective (LaVisionBiotec). ImSpector software was used to control the 2PM system and acquire images. Some image series were obtained with the help of an automated system providing real-time drift correction (39). Excitation was provided by a Ti:sapphire laser (Mai Tai HP, Spectraphysics) tuned to 780 or 840 nm. For analysis of cell migration, 11 to 20 x-y slices with a z-step size of 2-4 μm (22-64 μm depth) were acquired. Frame rate was 3 per min for LN or 1 per min for skin. Second

harmonic signals and emitted light were detected with 447/55-nm, 525/50-nm, 593/40-nm and 655/40-nm bandpass filters using non-descanned detectors. Image series were rendered into four-dimensional videos with Imaris (Bitplane) or Volocity (PerkinElmer) software. Tissue movement was corrected by either the correct drift function of Imaris or with a MATLAB script identifying the 3D movement in a reference channel. Motility parameters such as angle changes were derived from x, y, and z coordinates of cell centroids using Imaris, Volocity and MATLAB protocols. The cutoff for the arrest coefficient in LN was 5 μm/min and in epidermis 1 μm/min. Motility coefficients, which are a measure of a randomly moving cell's ability to move away from its starting position, were calculated from the slope of a graph of the average mean displacement against the square root of time. Shape factor was calculated by analyzing 2D projections of cell tracks of horizontally moving cells in Volocity as described (40). For some depicted image series, raw cell signals were masked with Imaris to hide autofluorescence. Brightness and contrast were adjusted in all images.

Statistical analysis

Unpaired Student's test, Mann-Whitney test, or Two-way ANOVA with a Sidak's multiple comparison test were used to determine statistical significance as indicated (Prism 7, GraphPad). Significance was set at $p < 0.05$.

Results

In vitro characterization of naive Flot1$^{-/-}$ T cells

Flot1 is a ubiquitously expressed, evolutionary conserved lipid-raft-associated protein, which accumulates at uropods of neutrophils and primary T cells (Fig. 1A) (18). RNAseq data from the Immgen database (www.immgen.org) revealed Flot1 expression in murine CD8$^+$ T cells throughout an immune response (Fig. 1B). We decided to analyze the role of Flot1 for CD8$^+$ T cell migration and activation. Western blot analysis confirmed the loss of Flot1 expression in Flot1$^{-/-}$ T cells and a concomitant decrease of Flot2 as described for Flot1$^{-/-}$ neutrophils (Fig. 1C) (24). In fibroblasts lacking Flot1, the remaining pool of Flot2 is not associated with lipid rafts, in line with a role for heterodimers or hetero-oligomers for proper membrane microdomain localization (24). We investigated the distribution of Flot2 in CCL21-polarized WT and Flot1$^{-/-}$ T cells by immunofluorescence. We confirmed Flot2 capping at the tip of uropods in WT T cells, whereas residual Flot2 showed a more uniform distribution in Flot1$^{-/-}$ T cells (Fig. 1D and 1E).

Polyclonal Flot1$^{-/-}$ CD8$^+$ T cells isolated from lymphoid organs displayed a *bona fide* naïve CD62L^{high} CD44^{low} phenotype and showed comparable levels of surface CCR7, indicating that T_N were predominant in secondary lymphoid organs (SLOs) (Fig. 1F and 1G and not shown). We compared the *in vitro* ability of naïve and activated WT and Flot1$^{-/-}$ T cells to polarize after chemokine stimulation. Flot1 accumulated in the uropod of polarized murine T cells (Supplemental Fig. 1), comparable to findings in human T cells. Activated Flot1$^{-/-}$ T cell blasts but not naïve Flot1$^{-/-}$ T cells showed a minor tendency to polarize less and to accumulate less pERM at the uropod as compared to WT blasts (Fig. 1H-J). We next analyzed the chemotactic ability of WT and Flot1$^{-/-}$ T_N towards CCL21 across 3 μm and 5

μm pore size filters. In line with their largely intact polarization, both cell types migrated similarly towards CCL21 (Fig. 1K).

We addressed whether residual Flot2 may compensate for Flot1 during *in vitro* migration. Flot2$^{-/-}$ splenocytes lacked expression of Flot2 as predicted and displayed essentially no detectable Flot1, in line with the mutually stabilizing role of both proteins (Supplemental Fig. 2A). Nonetheless, WT and Flot2$^{-/-}$ splenocytes showed comparable chemotaxis to CCL21 across 3 μm and 5 μm pore size filters (Supplemental Fig. 2B).

Since lipid raft-associated flotillin hetero-oligomers have been implicated in cortical actin binding, we hypothesized that Flot1 could influence membrane tension or membrane-to-cortex attachment. We therefore measured the membrane tension by pulling membrane tethers from the surface of activated WT and Flot1$^{-/-}$ T cell blasts using a cantilever on an atomic force microscope (Fig. 1L). Lack of Flot1 did not alter the static tether force as compared to WT T cells (Fig. 1M). In sum, lack of Flot1 has no major impact on membrane tension, nor on the ability of T cells to polarize and migrate in response to homeostatic chemokines.

In vivo characterization of naïve Flot1$^{-/-}$ T cell migration in lymphoid tissue

We next assessed whether Flot1 deficiency affects T cell trafficking under physiological conditions, which are difficult to reproduce in reductionist *in vitro* assays. To this end, we co-transferred WT and Flot1$^{-/-}$ CD8^{+} T$_N$ on an OT-I background into recipient mice for homing and intravital microscopy. OT-I T cells recognize the amino acid sequence SIINFEKL derived from Ovalbumin (OVA) in the context of H2-K^{b} (30). We recovered comparable numbers of WT and Flot1$^{-/-}$ CD8^{+} T cells from SLOs at 2 and 24 h after transfer (Fig. 2A and not shown), suggesting similar homing capacity of both cell types. To analyze interstitial migration in SLOs, we co-transferred WT dsRed^{+} and Flot1$^{-/-}$ GFP^{+} CD8^{+} T$_N$ into recipient mice and performed intravital 2PM imaging of the popliteal lymph node (PLN). Consistent with the T cell homing results, we observed both cell types inside the PLN interstitium (Fig. 2B). Time lapse imaging uncovered robust amoeboid motility WT and Flot1$^{-/-}$ CD8^{+} T cells (Fig. 2B and 2C; Supplemental Video 1). To quantify cell polarization, we determined the shape factor of migrating cells as described (40). A shape factor of 1 corresponds to a perfect circle, while values close to zero correlate to elongated or irregular shape outlines. Our analysis showed that Flot1$^{-/-}$ CD8^{+} T$_N$ displayed significantly rounder shapes as compared to WT CD8^{+} T cells (Fig. 2D). This correlated with a minor but significant drop in median cell speeds (from 13.5 ± 4.0 μm/min for WT CD8^{+} T$_N$ to 13.0 ± 4.1 μm/min for Flot1$^{-/-}$ CD8^{+} T$_N$; mean ± SD) (Fig. 2E). Yet, the arrest coefficient, defined as percent of track length with speeds slower than a defined threshold value, and the meandering index were comparable between both populations (Fig. 2F and 2G). Furthermore, both WT and Flot1$^{-/-}$ CD8^{+} T$_N$ preferentially change direction with shallow turning angles (~ 30°) while steep turns (~ 90°) or U-turns (~ 180°) were rare (not shown). Both persistence and speed contribute to the motility coefficient, which measures the displacement of randomly migrating cells over time and is calculated from plotting mean displacement versus time. WT and Flot1$^{-/-}$ CD8^{+} T$_N$ display comparable motility coefficients of 54.0 and 50.9 μm^2/min, respectively (Fig. 2H). In sum, interstitial Flot1$^{-/-}$ T

cells are more rounded than their WT counterparts and show a minor speed drop, which did not significantly hinder them to scan the lymphoid microenvironment *in vivo*.

Activation, expansion and memory formation of Flot1$^{-/-}$ CD8^{+} T cells

Flotillin-rich lipid rafts have been implicated in TCR signaling at the IS, contributing to T cell activation *in vitro* (27–29). In contrast, activation and memory formation of Flot1$^{-/-}$ CD8^{+} T cells has not been systematically analyzed *in vivo* to date. To explore this further, we adoptively transferred either GFP^{+} WT or GFP^{+} Flot1$^{-/-}$ OT-I T cells into recipient mice. At 24 h post transfer, we induced a systemic infection by i.p. injection of OVA-encoding Lymphocytic Choriomeningitis Virus (LCMV-OVA) (Fig. 3A) (38). We observed a comparable clonal expansion of WT OT-I and Flot1$^{-/-}$ OT-I T cells during the acute phase (day 6 p.i.), followed by a contraction after the effector phase (day 15 p.i.) and the formation of a long-lived memory pool (> day 28 p.i.) in lymphoid tissue and SMG (Fig. 3B). In the effector phase, activated CD8^{+} T cells differentiate from KLRG-1^{-} CD127^{-} early effector cells (EEC) into KLRG-1^{+} CD127^{-} short-lived effector cells (SLEC) or KLRG-1^{-} CD127^{+} memory precursor cells (MPEC), with few KLRG-1^{+} CD127^{+} double-positive effector cells (DPEC) (41). The decision of becoming SLEC versus MEPC is influenced by the strength of antigenic stimulation and the cytokine milieu and serves as readout for alterations in CD8^{+} T cell responsiveness. When we examined WT and Flot1$^{-/-}$ OT-I T cells on day 6 p.i., we observed most cells to be KLRG-1^{-} CD127^{-} EECs or KLRG-1^{+} CD127^{-} SLECs without notable changes in population ratios between WT or Flot1$^{-/-}$ OT-I T cells, indicating comparable activation (Fig. 3C and 3D).

Finally, we analyzed whether T_{RM} formation in SMG is affected by absence of Flot1. Both WT OT-I and Flot1$^{-/-}$ OT-I T cells exhibited a comparable gradual increase of the T_{RM} marker CD103 in SMG but not PLN or spleen, suggesting largely preserved capacity to form *bona fide* T_{RM} in non-lymphoid organs in the absence of Flot1 (Fig. 3E and 3F). Taken together, our data suggest normal clonal expansion, differentiation, tissue infiltration and memory formation of Flot1$^{-/-}$ CD8^{+} T cells during an antiviral immune response.

In vivo migration of Flot1$^{-/-}$ CD8^{+} memory T cells in lymphoid tissue

We set out to examine the tissue surveillance properties of memory CD8^{+} T cells in lymphoid tissue after viral infections. To this end, we co-transferred dsRed^{+} WT OT-I and GFP^{+} Flot1$^{-/-}$ OT-I CD8^{+} T cells into recipient mice, which were infected with LCMV-OVA one day later. After > day 30 p.i., we performed intravital imaging of PLN (Fig. 4A). Both WT OT-I and Flot1$^{-/-}$ OT-I T cells displayed active amoeboid migration in the PLN interstitium, similar to T_N (Fig. 4B and 4C; Supplemental Video 2). Compared to memory OT-I T cells, Flot1$^{-/-}$ T cells were on average rounder than their WT counterparts (Fig. 4D). This correlated to a minor, but statistically significant reduction in migration speeds of memory Flot1$^{-/-}$ OT-I T cells as compared to WT OT-I T cells (from 11.2 ± 3.9 μm/min for WT memory CD8^{+} T cells to 10.2 ± 3.7 μm/min for Flot1$^{-/-}$ memory CD8^{+} T cells; mean ± SD) (Fig. 4E). In addition, the arrest coefficient was increased in Flot1$^{-/-}$ memory OT-I T cells, while the meandering index of Flot1$^{-/-}$ memory T cells was slightly reduced as compared to WT OT-I T cells (Fig. 4F and 4G). As a consequence, Flot1$^{-/-}$ memory T cells displayed a reduced motility coefficient compared to WT memory T cells (54.3 versus 34.8

μm^2/min for WT and Flot1$^{-/-}$ CD8$^+$ T cells, respectively; Fig. 4H). Thus, Flot1 plays a detectable role in the morphology and migration of lymphoid tissue memory CD8$^+$ T cells, which mostly consist of T_{CM}. Nonetheless, the ability of CD8$^+$ T cells lacking Flot1 to scan the lymphoid microenvironment remains comparably robust.

Patrolling behavior of Flot1$^{-/-}$ CD8$^+$ T_{RM} in epidermis

Since uropod function is critical in dense environments for nuclear propulsion and Flot1 is required for neutrophil accumulation in non-lymphoid tissue (11, 24, 42, 43), we reasoned that the function of Flot1-mediated control of cell shape may become more apparent in dense non-lymphoid tissue. To address this point experimentally, we co-transferred GFP$^+$ Flot1$^{-/-}$ OT-I and dsRed$^+$ WT OT-I T cells into WT recipients and performed skin tattooing of a tandem dimer Tomato- and OVA-encoding Herpes Simplex Virus-1 ($HSV_{TOM-OVA}$) one day later as described (Fig. 5A) (6). In this setting, viral infections lead to the recruitment of CD8$^+$ effector T cells, which differentiate after viral clearance into epidermal T_{RM} (38). Similar to our findings in the LCMV-OVA infection model, lack of Flot1 did not impair effector cell recruitment to skin by day 7 p.i., suggesting a preserved capacity of Flot1$^{-/-}$ CD8$^+$ T cells to switch from lymphoid to non-lymphoid tissue infiltration (Fig. 5B). We furthermore observed a largely preserved maintenance of OT-I and Flot1$^{-/-}$ OT-I populations in spleen, skin-draining axillary and inguinal LN (dLN) and skin by flow cytometry at > day 28 p.i. (Supplemental Fig. 3A). In line with this observation, the ratio of % OT-I T cell populations (among CD45$^+$ CD8$^+$ cells) in skin versus dLN of individual mice remained comparable for both OT-I and Flot1$^{-/-}$ OT-I T cells, suggesting a similar distribution of T_{RM} and T_{CM} in both populations (Supplemental Fig. 3B).

At 5 weeks p.i., we surgically prepared the tattooed skin for intravital imaging of WT and Flot1$^{-/-}$ T_{RM}. Epidermal T_{RM} are located within the basal epidermis above a loose layer of dermal collagen, which can be visualized in 2PM by second harmonic generation. Within the dense epithelial microenvironment, epidermal T_{RM} migrate at 1 - 2 μm/min while displaying a highly dendritic morphology with many finger-like protrusions (44, 45). We observed that both WT and Flot1$^{-/-}$ T_{RM} exhibit this typical morphology and epidermal localization (Fig. 5C and 5D; Movie S3). Shape factors of both WT and Flot1$^{-/-}$ epidermal T_{RM} were much lower than of lymphoid tissue T cells, reflecting their highly elongated morphology. In contrast to Flot1$^{-/-}$ T cells in lymphoid organs, epidermal Flot1$^{-/-}$ T_{RM} displayed a significantly more elongated morphology as compared to WT cells (Fig. 5E). WT epidermal T_{RM} migrated with a mean speed of 1.7 ± 0.7 μm/min, while Flot1$^{-/-}$ epidermal T_{RM} migrated with a reduced speed of 1.4 ± 0.6 μm/min (mean ± SD) (Fig. 5F). Furthermore, Flot1$^{-/-}$ T_{RM} had a higher arrest coefficient, but a similarly low meandering index as WT T_{RM} (Fig. 5G and 5H). Despite these minor changes in cell motility parameters, the motility coefficient of epidermal Flot1$^{-/-}$ epidermal T_{RM} was unchanged compared to WT T_{RM} (Fig. 5I). In conclusion, Flot1$^{-/-}$ epidermal T_{RM} retain the capacity of scanning even a very dense microenvironment consisting of epithelial layers.

Secondary expansion of WT and Flot1$^{-/-}$ memory CD8$^+$ T cells after microbial challenge

Finally, we set out to examine whether Flot1 deficiency interferes with a secondary expansion of memory CD8$^+$ T cells. We generated mice containing WT and Flot1$^{-/-}$ memory

OT-I T cells at > 30 days post LCMV-OVA infection, which were then re-challenged with OVA-expressing Listeria monocytogenes (Lm-OVA) (Fig. 6A). At day 4 p.i., we isolated spleens and examined secondary expansion by flow cytometry (Fig. 6B). We found that both populations expanded equally well following Lm-OVA challenge (Fig. 6C). Similarly, OT-I and Flot1$^{-/-}$ OT-I T cells expressed similar levels of KLRG-1, a marker which is upregulated upon secondary challenge (not shown) (46). Taken together, our data suggest that CD8^{+} memory T cells retain a comparable capacity for secondary expansion in the absence of Flot1 expression in ou experimental system.

Discussion

CD8^{+} T cells are remarkably efficient in scanning a wide variety of target tissues in search of pMHC-presenting DCs and target cells. To this end, these cells acquire a polarized shape with protrusive and contracting membrane dynamics. Flot1 is a highly conserved protein that scaffolds lipid rafts and controls the cortical cytoskeleton of neutrophil uropods, where it accumulates (24). Yet, its *in vivo* function for adaptive immune cell trafficking and activation has not been explored to date. Our data uncover a role for Flot1 in regulating CD8^{+} T cell speeds in lymphoid and non-lymphoid tissues. Furthermore, Flot1 contributes to shape maintenance but does not affect expansion during a primary and secondary immune response under the experimental conditions used here.

Flotillins are involved in TCR recycling and signaling at the IS (27, 29). Yet, in our system using a transgenic TCR (OT-I) and cognate peptide expressed by replication-competent viruses, we did not observe a defect in expansion, MPEC versus SLEC differentiation and memory formation of Flot1$^{-/-}$ CD8^{+} T cells. Similarly, dissemination of effector and memory Flot1$^{-/-}$ CD8^{+} T cells to lymphoid and non-lymphoid tissue was comparable to WT CD8^{+} T cells. We assessed effector T cell numbers and phenotypes at day 6 post infection, which may have been too late to detect alterations during early T cell activation. It is also possible that the strong affinity of OT-I to its cognate peptide-MHC is sufficient to override Flot1-mediated defects or that T cells compensate for lower signaling strength by a longer interaction time with DCs. Furthermore, residual Flot2 levels may have partially rescued the lack of Flot1 expression. Yet, Flot1 expression has been reported to be required for lipid raft localization of Flot2 (24). Similarly, we observed altered Flot2 expression in polarized Flot1$^{-/-}$ lymphocytes. While these data support the notion that lack of Flot1 abolishes the formation of functional hetero-oligomers, Flot2 retains F-actin binding activity, which may be sufficient to fulfil Flot1-independent functions. In addition, other proteins contributing to uropod formation such as ERM proteins may also compensate for the lack of flotillin hetero-oligomers (35).

We used 2PM imaging of PLN and skin to asses morphology and migratory patterns of Flot1$^{-/-}$ CD8^{+} T cells in *vivo*. We consistently found changes in cell shape: Lymphoid tissue Flot1$^{-/-}$ T cells were less elongated than their WT counterparts, while the opposite was observed for epidermal T_{RM}. This may reflect the distinct modes of motility imposed by the microenvironment of these tissues. Lymphoid tissue T cells display amoeboid cell motility, which is characterized by a polarized cell shape with an F-actin rich leading edge and a well-developed uropod containing myosin II. Our *in vivo* observations of naïve and memory

T cell shapes in lymphoid tissue confirm previous *in vitro* studies showing impaired uropod formation in primary T cells upon expression of a dominant-negative Flot2 mutant or suppression of Flot1 expression (18, 22, 35). In contrast, epidermal T_{RM} display a highly branched morphology and use a finger-like migration mode. It was hypothesized that actin-polymerization is driving the extension of the finger, while myosin-mediated contractility is required for contraction of the protrusion and for cell translocation (47). Therefore, a minor reduction in myosin contractility through lack of Flot1-mediated microdomain assembly may explain the hyperelongated protrusions of epidermal T_{RM}. Nonetheless, we could not find consistent evidence that hyperelongation resulted in cell disintegration in Flot1$^{-/-}$ T_{RM} (not shown). Taken together, Flot1-containing microdomains shape T cell morphology *in vivo* but are not absolutely required for cell displacement and maintenance of cellular integrity in the experimental conditions examined here.

RNAseq expression levels of Flot1 and lipid raft content are comparable between naïve and memory CD8$^+$ T cells (48). However, multiple interacting partners of flotillins, such as the adhesion molecule CD44, are differentially expressed in naïve versus memory CD8$^+$ T cells. Changes in the interactome of Flot1 may therefore underlie the larger impact of Flot1 deficiency on lymph node memory CD8$^+$ T cell motility as compared to T_N. Similarly, Flot1$^{-/-}$ epidermal T_{RM} migrated with a slower velocity compared to WT T_{RM}. Despite these minor changes in cell shape and motility parameters, our data suggest that Flot1 plays a less prominent role in CD8$^+$ T cells as compared to neutrophils and monocytes (24). This may be due to the fact that while readily detectable by gene expression and western blot, Flot1 expression levels are several times lower in T cells as compared to neutrophils (www.immgen.org).

In sum, the present data demonstrate that Flot1$^{-/-}$ CD8$^+$ T cells are capable of expansion and formation of effector and memory T cells following viral infection. Furthermore, our imaging experiments show that morphology and homeostatic immune surveillance by CD8$^+$ T cells in lymphoid and non-lymphoid tissue is affected but not critically impaired by the absence of Flot1. Thus, while flotillins are evolutionary conserved and ubiquitously expressed, we demonstrate here that their function is regulated in a context- and cell type-specific manner, potentially reflecting expression levels and interaction partners.

Supplementary Material

Refer to Web version on PubMed Central for supplementary material.

Acknowledgements

This work benefitted from optical setups of the Microscopy Imaging Center of the University of Bern and the Bioimaging platform of the University of Fribourg.

Financial support

This work was funded by Swiss National Foundation (SNF) project grants 31003A_135649, 31003A_153457 and 31003A_172994 (to JVS), 31003A_169936 (to DFL), the European Molecular Biology Laboratory (to ADM), Leopoldina fellowship LPDS 2011-16 and SFB1129 (to BS).

References

1. Iijima N, Iwasaki A. A local macrophage chemokine network sustains protective tissue-resident memory CD4 T cells. Science. 2014; 346:93–98. [PubMed: 25170048]
2. Schenkel JM, Fraser KA, Beura LK, Pauken KE, Vezys V, Masopust D. Resident memory CD8 T cells trigger protective innate and adaptive immune responses. Science. 2014; 346:98–101. [PubMed: 25170049]
3. Stary G, Olive A, Radovic-Moreno AF, Gondek D, Alvarez D, Basto PA, Perro M, Vrbanac VD, Tager AM, Shi J, Yethon JA, et al. A mucosal vaccine against Chlamydia trachomatis generates two waves of protective memory T cells. Science. 2015; 348
4. Ariotti S, Hogenbirk MA, Dijkgraaf FE, Visser LL, Hoekstra ME, Song J-Y, Jacobs H, Haanen JB, Schumacher TN. Skin-resident memory $CD8^+$ T cells trigger a state of tissue-wide pathogen alert. Science. 2014; 346:101–105. [PubMed: 25278612]
5. Kadoki M, Patil A, Thaiss CC, Brooks DJ, Pandey S, Deep D, Alvarez D, von Andrian UH, Wagers AJ, Nakai K, Mikkelsen TS, et al. Organism-Level Analysis of Vaccination Reveals Networks of Protection across Tissues. Cell. 2017:1–38.
6. Ariotti S, Beltman JB, Borsje R, Hoekstra ME, Halford WP, Haanen JBAG, de Boer RJ, Schumacher TNM. Subtle CXCR3-Dependent Chemotaxis of CTLs within Infected Tissue Allows Efficient Target Localization. The Journal of Immunology. 2015; 195:5285–5295. [PubMed: 26525288]
7. Zaid A, Hor JL, Christo SN, Groom JR, Heath WR, Mackay LK, Mueller SN. Chemokine Receptor-Dependent Control of Skin Tissue-Resident Memory T Cell Formation. The Journal of Immunology. 2017; 199:2451–2459. [PubMed: 28855310]
8. Lämmermann T, Sixt M. Mechanical modes of “amoeboid” cell migration. Current Opinion in Cell Biology. 2009; 21:636–644. [PubMed: 19523798]
9. Krummel MF, Macara I. Maintenance and modulation of T cell polarity. Nat Immunol. 2006; 7:1143–1149. [PubMed: 17053799]
10. Moreau HD, Piel M, Voituriez R, Lennon-Duménil A-M. Integrating Physical and Molecular Insights on Immune Cell Migration. Trends Immunol. 2018:1–12.
11. Friedl P, Weigelin B. Interstitial leukocyte migration and immune function. Nat Immunol. 2008; 9:960–969. [PubMed: 18711433]
12. Vicente-Manzanares M, Ma X, Adelstein RS, Horwitz AR. Non-muscle myosin II takes centre stage in cell adhesion and migration. Nat Rev Mol Cell Biol. 2009; 10:778–790. [PubMed: 19851336]
13. Morin NA, Oakes PW, Hyun Y-M, Lee D, Chin YE, King MR, Springer TA, Shimaoka M, Tang JX, Reichner JS, Kim M. Nonmuscle myosin heavy chain IIA mediates integrin LFA-1 de-adhesion during T lymphocyte migration. J Exp Med. 2008; 205:195–205. [PubMed: 18195072]
14. Jacobelli J, Friedman RS, Conti MA, Lennon-Duménil A-M, Piel M, Sorensen CM, Adelstein RS, Krummel MF. Confinement-optimized three-dimensional T cell amoeboid motility is modulated via myosin IIA–regulated adhesions. Nat Immunol. 2010; 11:953–961. [PubMed: 20835229]
15. Niggli, V. Insights into the Mechanism for Dictating Polarity in Migrating T-CellsInternational Review of Cell and Molecular Biology. Vol. 312. Elsevier; 2014. 201–270.
16. Babuke T, Tikkanen R. Dissecting the molecular function of reggie/flotillin proteins. European Journal of Cell Biology. 2007; 86:525–532. [PubMed: 17482313]
17. Morrow IC, Parton RG. Flotillins and the PHB Domain Protein Family: Rafts, Worms and Anaesthetics. Traffic. 2005; 6:725–740. [PubMed: 16101677]
18. Affentranger S, Martinelli S, Hahn J, Rossy J, Niggli V. Dynamic reorganization of flotillins in chemokine- stimulated human T-lymphocytes. BMC Cell Biol. 2011; 12:28. [PubMed: 21696602]
19. Bodin S, Planchon D, Rios Morris E, Comunale F, Gauthier-Rouvière C. Flotillins in intercellular adhesion - from cellular physiology to human diseases. J Cell Sci. 2014; 127:5139–5147. [PubMed: 25413346]
20. Otto GP, Nichols BJ. The roles of flotillin microdomains - endocytosis and beyond. J Cell Sci. 2011; 124:3933–3940. [PubMed: 22194304]

21. Langhorst MF, Solis GP, Hannbeck S, Plattner H, Stuermer CAO. Linking membrane microdomains to the cytoskeleton: Regulation of the lateral mobility of reggie-1/flotillin-2 by interaction with actin. FEBS Letters. 2007; 581:4697–4703. [PubMed: 17854803]
22. Baumann T, Affentranger S, Niggli V. Evidence for chemokine-mediated coalescence of preformed flotillin hetero-oligomers in human T-cells. Journal of Biological Chemistry. 2012; 287:39664–39672. [PubMed: 23012365]
23. Sugawara Y, Nishii H, Takahashi T, Yamauchi J, Mizuno N, Tago K, Itoh H. The lipid raft proteins flotillins/reggies interact with GÎ±q and are involved in Gq-mediated p38 mitogen-activated protein kinase activation through tyrosine kinase. 2007; 19:1301–1308.
24. Ludwig A, Otto GP, Riento K, Hams E, Fallon PG, Nichols BJ. Flotillin microdomains interact with the cortical cytoskeleton to control uropod formation and neutrophil recruitment. J Cell Biol. 2010; 191:771–781. [PubMed: 21059848]
25. Baumann T, Affentranger S, Niggli V. Analysis of close associations of uropod-associated proteins in human T-cells using the proximity ligation assay. PeerJ. 2013; 1:e186–14. [PubMed: 24167781]
26. Giri B, Dixit VD, Ghosh MC, Collins GD, Khan IU, Madara K, Weeraratna AT, Taub DD. CXCL12-induced partitioning of flotillin-1 with lipid rafts plays a role in CXCR4 function. Eur J Immunol. 2007; 37:2104–2116. [PubMed: 17634952]
27. Slaughter N, Laux I, Tu X, Whitelegge J, Zhu X, Effros R, Bickel P, Nel A. The flotillins are integral membrane proteins in lipid rafts that contain TCR-associated signaling components: implications for T-cell activation. Clinical Immunology. 2003; 108:138–151. [PubMed: 12921760]
28. Langhorst MF, Reuter A, Luxenhofer G, Boneberg E-M, Legler DF, Plattner H, Stuermer CAO. Preformed reggie/flotillin caps: stable priming platforms for macrodomain assembly in T cells. The FASEB Journal. 2006; 20:711–713. [PubMed: 16452278]
29. Compeer EB, Kraus F, Ecker M, Redpath G, Amiezer M, Rother N, Nicovich PR, Kapoor-Kaushik N, Deng QG, Samson PB, Yang Z, et al. A mobile endocytic network connects clathrin-independent receptor endocytosis to recycling and promotes T cell activation. Nat Commun. 2018; 9:117–15. [PubMed: 29317616]
30. Hogquist KA, Jameson SC, Heath WR, Howard JL, Bevan MJ, Carbone FR. T cell receptor antagonist peptides induce positive selection. Cell. 1994; 76:17–27. [PubMed: 8287475]
31. Schaefer BC, Schaefer ML, Kappler JW, Marrack P, Kedl RM. Observation of antigen-dependent CD8+ T-cell/ dendritic cell interactions in vivo. Cell Immunol. 2001; 214:110–122. [PubMed: 12088410]
32. Kirby AC, Coles MC, Kaye PM. Alveolar Macrophages Transport Pathogens to Lung Draining Lymph Nodes. J Immunol. 2009; 183:1983–1989. [PubMed: 19620319]
33. Madisen L, Zwingman TA, Sunkin SM, Oh SW, Zariwala HA, Gu H, Ng LL, Palmiter RD, Hawrylycz MJ, Jones AR, Lein ES, et al. A robust and high-throughput Cre reporting and characterization system for the whole mouse brain. Nature Neuroscience. 2010; 13:133–140. [PubMed: 20023653]
34. de Vries WN, Binns LT, Fancher KS, Dean J, Moore R, Kemler R, Knowles BB. Expression of Cre recombinase in mouse oocytes: a means to study maternal effect genes. genesis. 2000; 26:110–112. [PubMed: 10686600]
35. Martinelli S, Chen EJH, Clarke F, Lyck R, Affentranger S, Burkhardt JK, Niggli V. Ezrin/Radixin/Moesin proteins and flotillins cooperate to promote uropod formation in T cells. Front Immun. 2013; 4:84.
36. Kallert SM, Darbre S, Bonilla WV, Kreutzfeldt M, Page N, ller PMU, Kreuzaler M, Lu M, Favre SEP, Kreppel F, hning MLO, et al. Replicating viral vector platform exploits alarmin signals for potent CD8+ T cell-mediated tumour immunotherapy. Nat Commun. 2017; 8:1–13. [PubMed: 28232747]
37. Zehn D, Lee SY, Bevan MJ. Complete but curtailed T-cell response to very low-affinity antigen. Nature. 2009; 458:211–214. [PubMed: 19182777]
38. Moalli F, Ficht X, Germann P, Vladymyrov M, Stolp B, de Vries I, Lyck R, Balmer J, Fiocchi A, Kreutzfeldt M, Merkler D, et al. The Rho regulator Myosin IXb enables nonlymphoid tissue seeding of protective CD8+ T cells. Journal of Experimental Medicine. 2018; 215:1869–1890. [PubMed: 29875261]

39. Vladymyrov M, Abe J, Moalli F, Stein JV, Ariga A. Real-time tissue offset correction system for intravital multiphoton microscopy. Journal of Immunological Methods. 2016; 438:35–41. [PubMed: 27589923]
40. Hons M, Kopf A, Hauschild R, Leithner A, Gaertner F, Abe J, Renkawitz J, Stein JV, Sixt M. Chemokines and integrins independently tune actin flow and substrate friction during intranodal migration of T cells. Nat Immunol. 2018; 19:606–616. [PubMed: 29777221]
41. Joshi NS, Cui W, Chandele A, Lee HK, Urso DR, Hagman J, Gapin L, Kaech SM. Inflammation Directs Memory Precursor and Short-Lived Effector CD8+ T Cell Fates via the Graded Expression of T-bet Transcription Factor. Immunity. 2007; 27:281–295. [PubMed: 17723218]
42. Nourshargh S, Hordijk PL, Sixt M. Breaching multiple barriers: leukocyte motility through venular walls and the interstitium. Nat Rev Mol Cell Biol. 2010; 11:366–378. [PubMed: 20414258]
43. Paluch EK, Aspalter IM, Sixt M. Focal Adhesion-Independent Cell Migration. Annu Rev Cell Dev Biol. 2016; 32:469–490. [PubMed: 27501447]
44. Ariotti S, Beltman JB, Chodaczek G, Hoekstra ME, van Beek AE, Gomez-Eerland R, Ritsma L, van Rheenen J, Marée AFM, Zal T, de Boer RJ, et al. Tissue-resident memory CD8+ T cells continuously patrol skin epithelia to quickly recognize local antigen. Proceedings of the National Academy of Sciences. 2012; 109:19739–19744.
45. Zaid A, Mackay LK, Rahimpour A, Braun A, Veldhoen M, Carbone FR, Manton JH, Heath WR, Mueller SN. Persistence of skin-resident memory T cells within an epidermal niche. Proc Natl Acad Sci USA. 2014; 111:5307–5312. [PubMed: 24706879]
46. Herndler-Brandstetter D, Ishigame H, Shinnakasu R, Plajer V, Stecher C, Zhao J, Lietzenmayer M, Kroehling L, Takumi A, Kometani K, Inoue T, et al. KLRG1+ Effector CD8+ T Cells Lose KLRG1, Differentiate into All Memory T Cell Lineages, and Convey Enhanced Protective Immunity. Immunity. 2018; 48:716–729.e8. [PubMed: 29625895]
47. Zhu J, Mogilner A. Comparison of cell migration mechanical strategies in three-dimensional matrices: a computational study. Interface Focus. 2016; 6:20160040–12. [PubMed: 27708764]
48. de Mello Coelho V, Nguyen D, Giri B, Bunbury A, Schaffer E, Taub DD. Quantitative differences in lipid raft components between murine CD4+ and CD8+ T cells. BMC Immunol. 2004; 5:2. [PubMed: 15005797]

Europe PMC Funders Author Manuscripts

Europe PMC Funders Author Manuscripts

Key points

- Flot1$^{-/-}$ CD8^{+} T cells have altered cell morphology and speeds *in vivo*
- Flot1$^{-/-}$ CD8^{+} T cells show robust expansion and infiltration of peripheral tissues

Europe PMC Funders Author Manuscripts

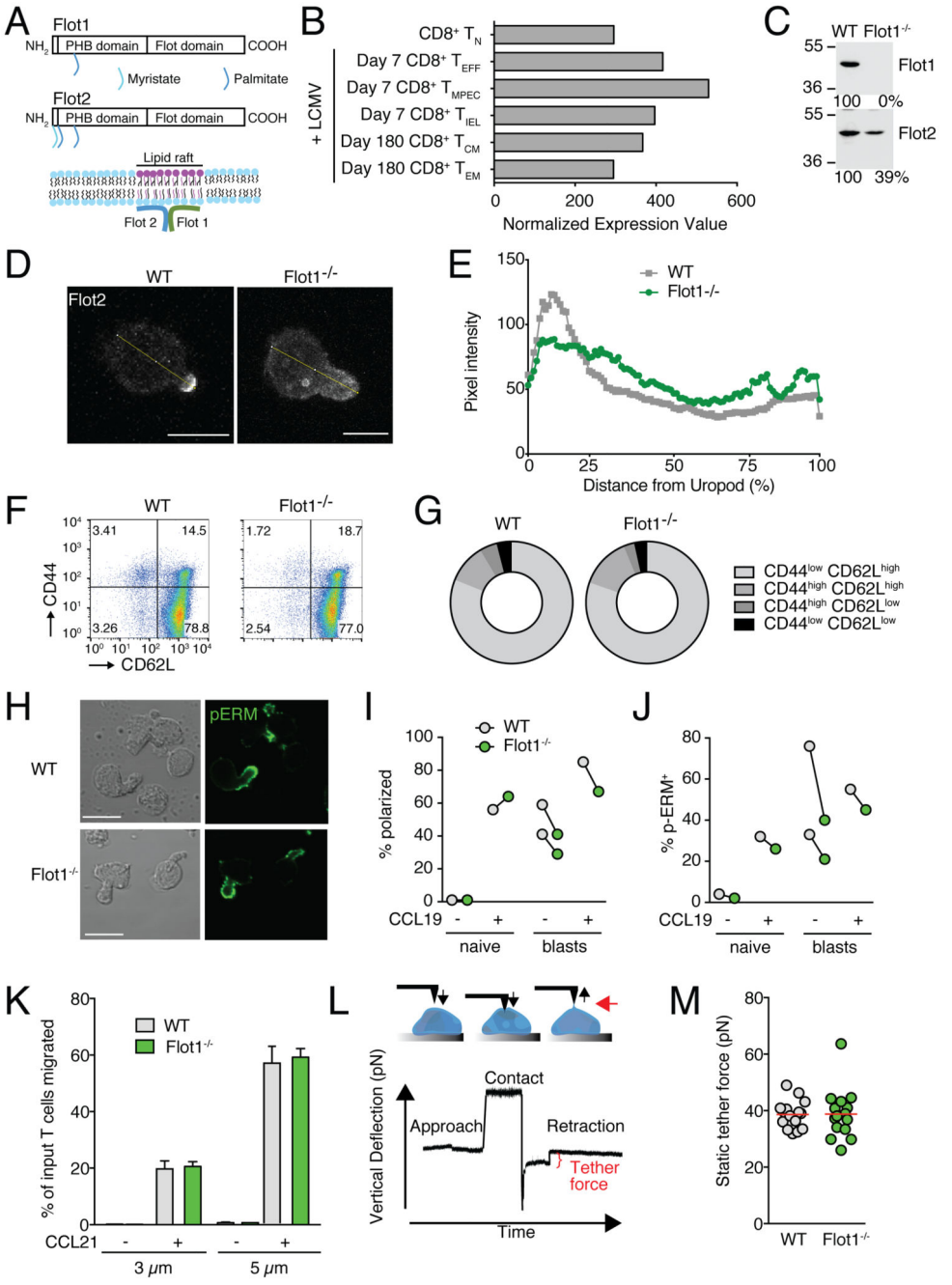

Figure 1. *In vitro* characterization of Flot1$^{-/-}$ T cells.

A. Scheme of Flot1 and Flot2 protein domains and association with lipid raft microdomains. PHB, prohibitin homology domain. **B.** RNA-seq data of Flot1 expression in CD8^{+} T cells (from Immgen database). **C.** Expression of Flot1 and Flot2 in T-lymphoblasts isolated from spleens of wild type and Flot1$^{-/-}$ mice. **D.** Immunofluorescent images of WT and Flot1$^{-/-}$ T cells stimulated with CCL21 and stained for Flot2. Yellow line depicts fluorescence intensity assessment. Scale bar, 5 μm. **E.** Flot2 pixel intensity per cell normalized to distance from uropod. n = 26 and 21 for WT and Flot1$^{-/-}$ T cells, respectively. **F**. Flow cytometry plot of

CD62L and CD44 expression on splenic $CD8^+$ T cells. **G.** Quantification of surface expression of CD44 and CD62L on $CD8^+$ T cells from WT and $Flot1^{-/-}$ mice. Pooled from 2 independent experiments, n = 4. **H.** Phase contrast and immunofluorescent images of polarized activated WT and $Flot1^{-/-}$ T cell blasts stimulated with CCL19 and stained for pERM. Scale bar, 10 μm. **I, J.** Quantification of polarization (I) and pERM capping (J) of naïve and activated T cells with and without CCL19 stimulation. **K.** Chemotaxis of naïve WT and $Flot1^{-/-}$ T cells towards 100 nM CCL21 through 3 and 5 μm filters. Shown is mean ± SD of one of two experiments performed in triplicates. **L.** Schematic of pulling static tethers with an atomic force microscope. **M.** Average static tether force per cell. Data shows one representative experiment of two.

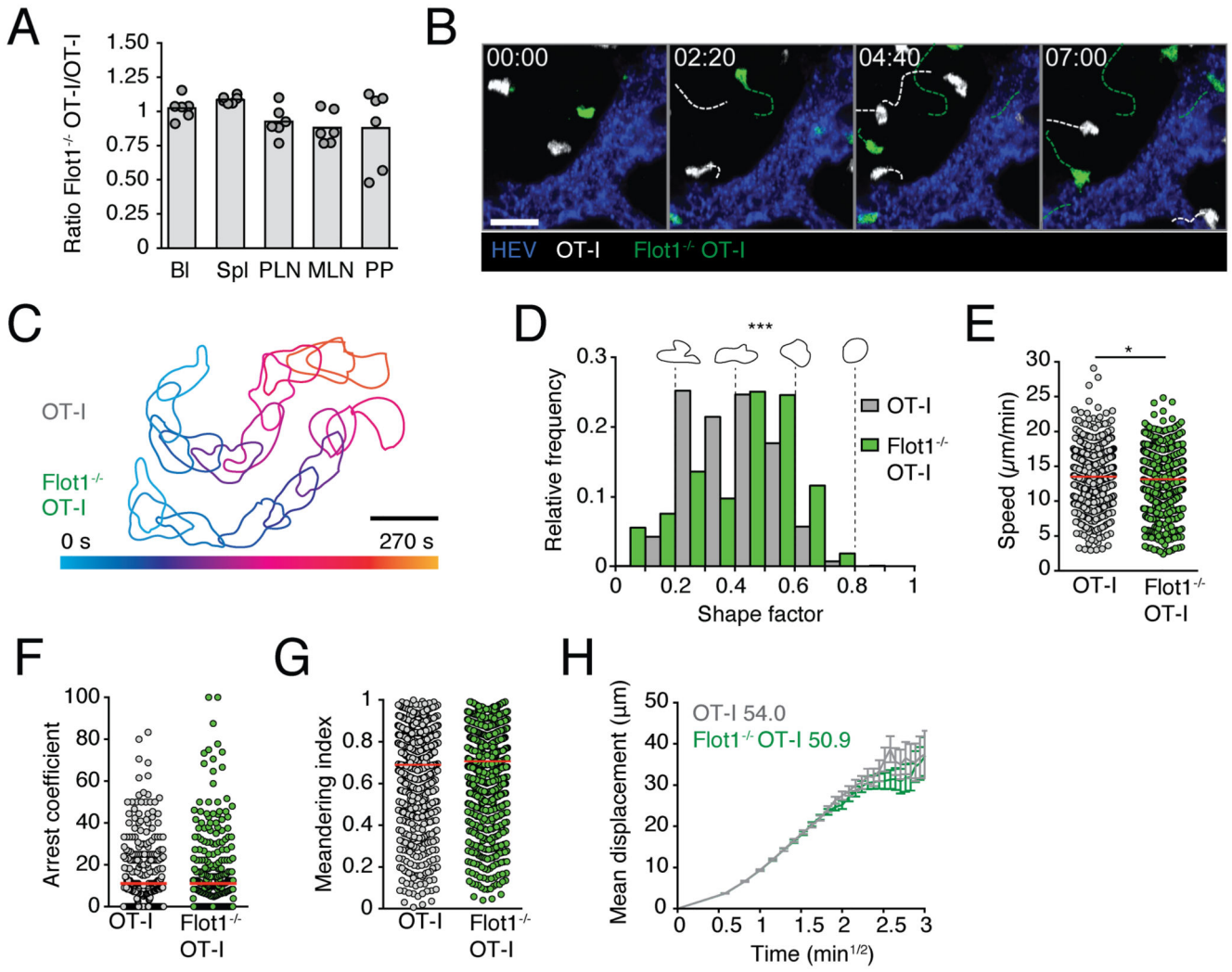

Figure 2. *In vivo* trafficking of naïve Flot1$^{-/-}$ CD8^{+} T cells in lymphoid organs.

A. 2 h *in vivo* homing of OT-I or Flot1$^{-/-}$ OT-I T cells to indicated organs: blood (Bl), spleen (Spl), peripheral lymph nodes (PLN), mesenteric lymph nodes (MLN) and Peyer's patches (PP). Each dot represents organs from one mouse, bars depict mean. Pooled from 2 independent experiments with a total of 6 mice per group. **B.** 2PM image sequence of naive WT and Flot1$^{-/-}$ OT-I T cells migrating in popliteal LN. Dashed white and green lines indicate tracks of migrating WT and Flot1$^{-/-}$ OT-I T cells, respectively. Scale bar, 20 μm; Time in min:s. **C.** Representative time-coded outlines of migrating WT and Flot1$^{-/-}$ OT-I T cells. Scale bar, 10 μm. **D.** Shape factor of naive WT and Flot1$^{-/-}$ OT-I T cells migrating in popliteal LN. Pooled from 2 independent experiments with 3 mice per group. **E-G.** Speed (E), arrest coefficient (F) and meandering index (G) of naïve WT or Flot1$^{-/-}$ OT-I T cells migrating in popliteal LN. Red lines depict median, each dot represents the average value for an individual track. **H.** Mean displacement versus time for datasets in E-G. Numbers indicate motility coefficient in μm^2/min. Data in E-H are pooled from 3 independent experiments with a total of 8 mice. Data in A were tested for significance with 2-way

ANOVA and Sidak's multiple comparison test. Data in E were analyzed using unpaired Student's t-test, data in D, F and G using Mann-Whitney test. *, $p < 0.05$; ***, $p < 0.001$.

Europe PMC Funders Author Manuscripts

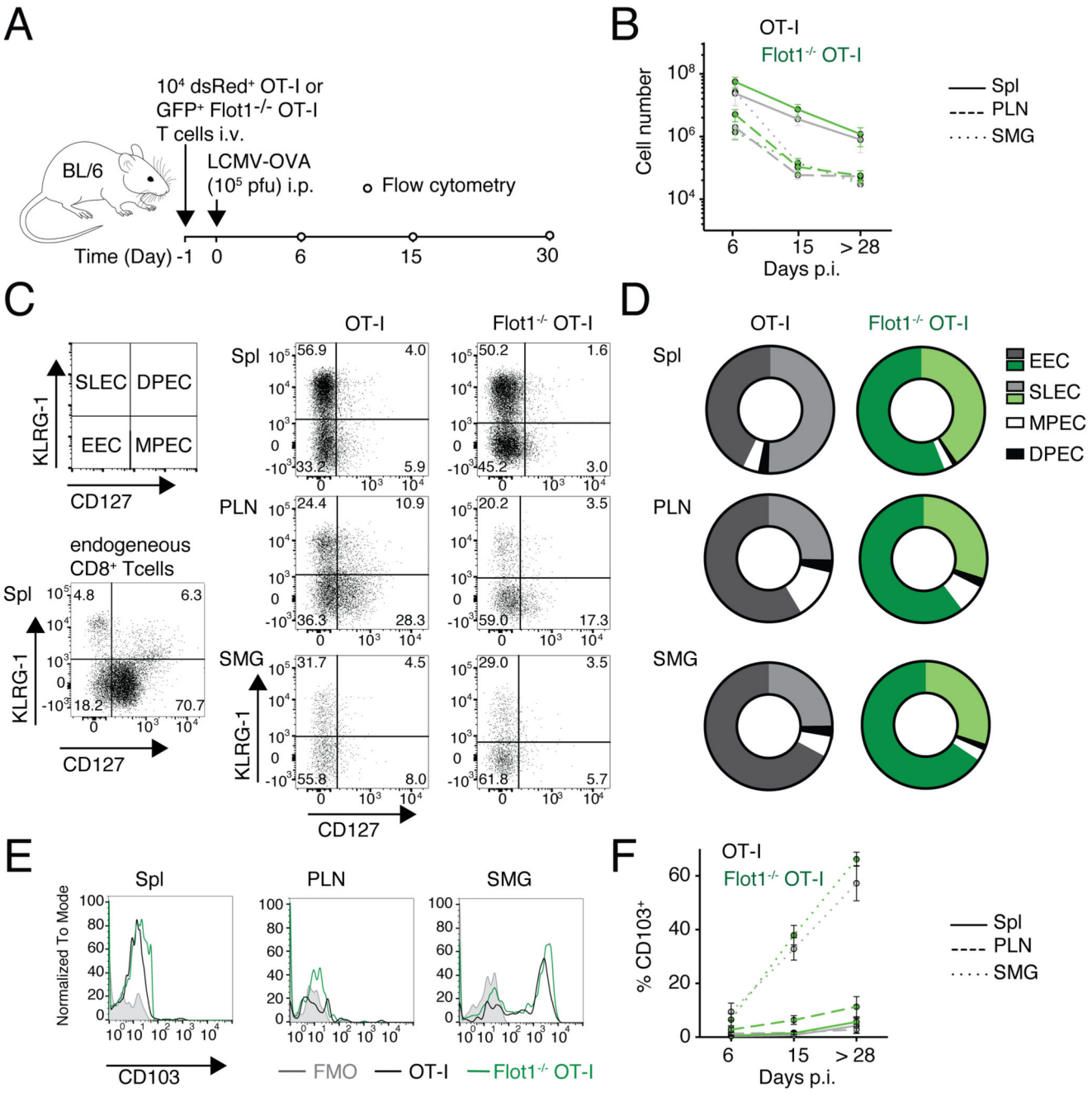

Figure 3. Expansion and memory formation of Flot1$^{-/-}$ CD8^{+} T cells.

A. Experimental layout of LCMV-OVA infection. **B.** Total number of GFP^{+} cell number in spleen (Spl), pooled peripheral lymph nodes (PLN) and submandibular salivary gland (SMG) at day 6, 15, and >28 p.i. Pooled from 2 independent experiments with a total of 5-6 mice per group. **C, D.** Representative flow cytometry plots (C) and pooled results (D) of CD127 and KLRG-1 co-staining of endogenous CD8^{+} and transferred OT-I T cells on 6 d p.i.. Pooled from 2 independent experiments and a total of 4-8 mice. **E, F.** Representative flow cytometry plots (E) and pooled results (F) of CD103 expression on OT-I and Flot1$^{-/-}$

Europe PMC Funders Author Manuscripts

OT-I T cells in memory phase (>28 days p.i.). F shows mean with SEM from 2-4 independent experiments with a total of 5-12 mice per group and time point.

Europe PMC Funders Author Manuscripts

Europe PMC Funders Author Manuscripts

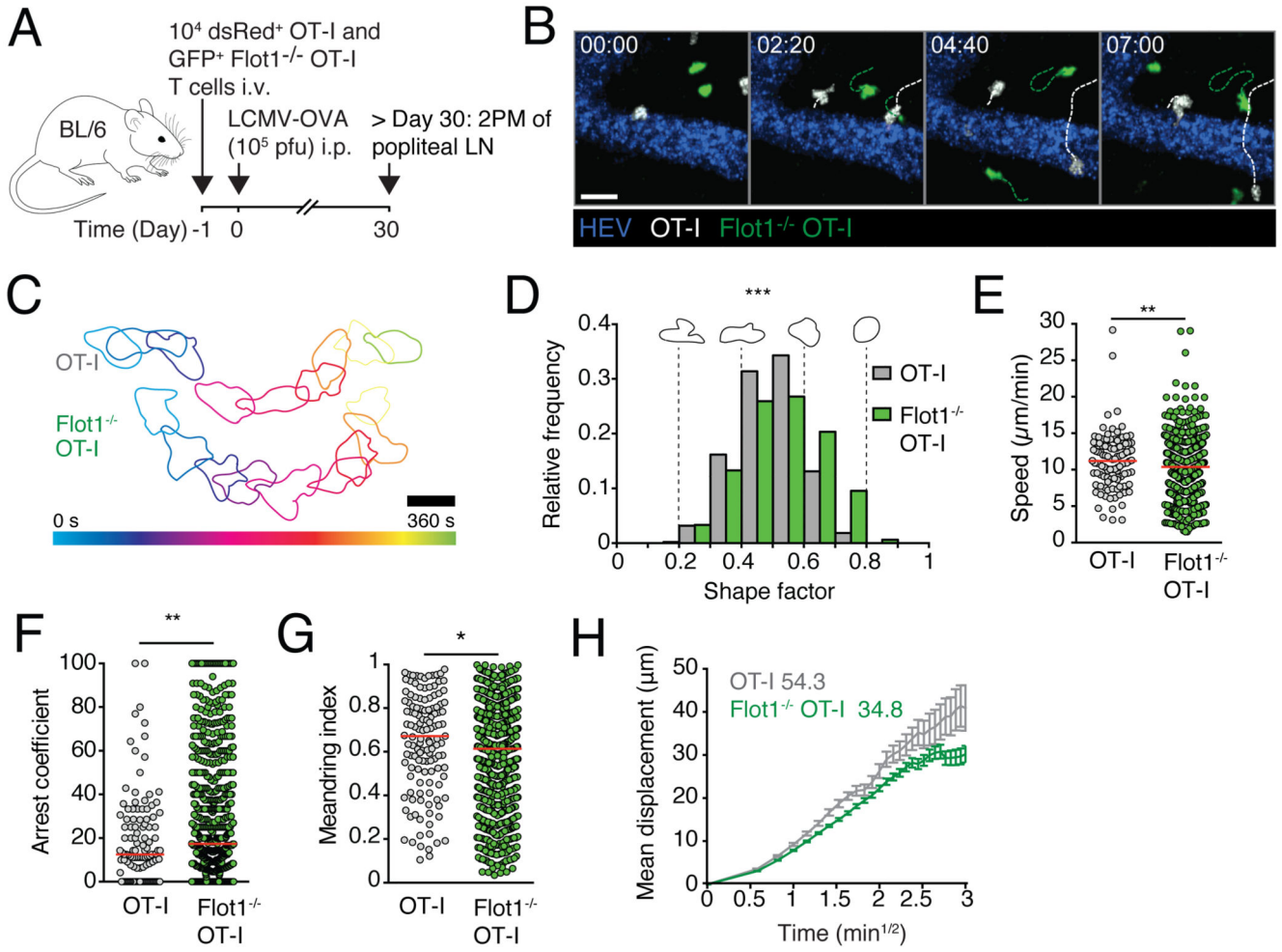

Figure 4. *In vivo* trafficking of memory Flot1$^{-/-}$ CD8^{+} T cells in lymphoid organs.

A. Experimental layout. **B.** 2PM image sequence of memory OT-I and Flot1$^{-/-}$ OT-I T cells migrating in popliteal LN. Dashed white and green lines indicate tracks of migrating memory OT-I and Flot1$^{-/-}$ OT-I T cells, respectively. Scale bar 20 μm; Time in min:s. **C.** Representative time-coded outlines of migrating memory OT-I and Flot1$^{-/-}$ OT-I T cells in PLN. Scale bar, 10 μm. **D.** Shape factor of memory OT-I and Flot1$^{-/-}$ OT-I T cells migrating in popliteal LN. Pooled from 2 independent experiments with 3 mice per group. **E-G.** Speed (E), arrest coefficient (F) and meandering index (G) of memory OT-I or Flot1$^{-/-}$ OT-I T cells migrating in LN. Red lines depict median, each dot represents the average value for an individual track. **H.** Mean displacement versus time for datasets in E-G. Numbers indicate motility coefficient in μm^2/min. Flot1$^{-/-}$ OT-I data in D-H are pooled from 3 independent experiments (n = 8) and OT-I data are pooled from 2 independent experiments (n = 5). Data in E were analyzed using unpaired Student's t-test, data in D, F and G using Mann-Whitney test. *, $p < 0.05$; **, $p < 0.01$; ***, $p < 0.001$.

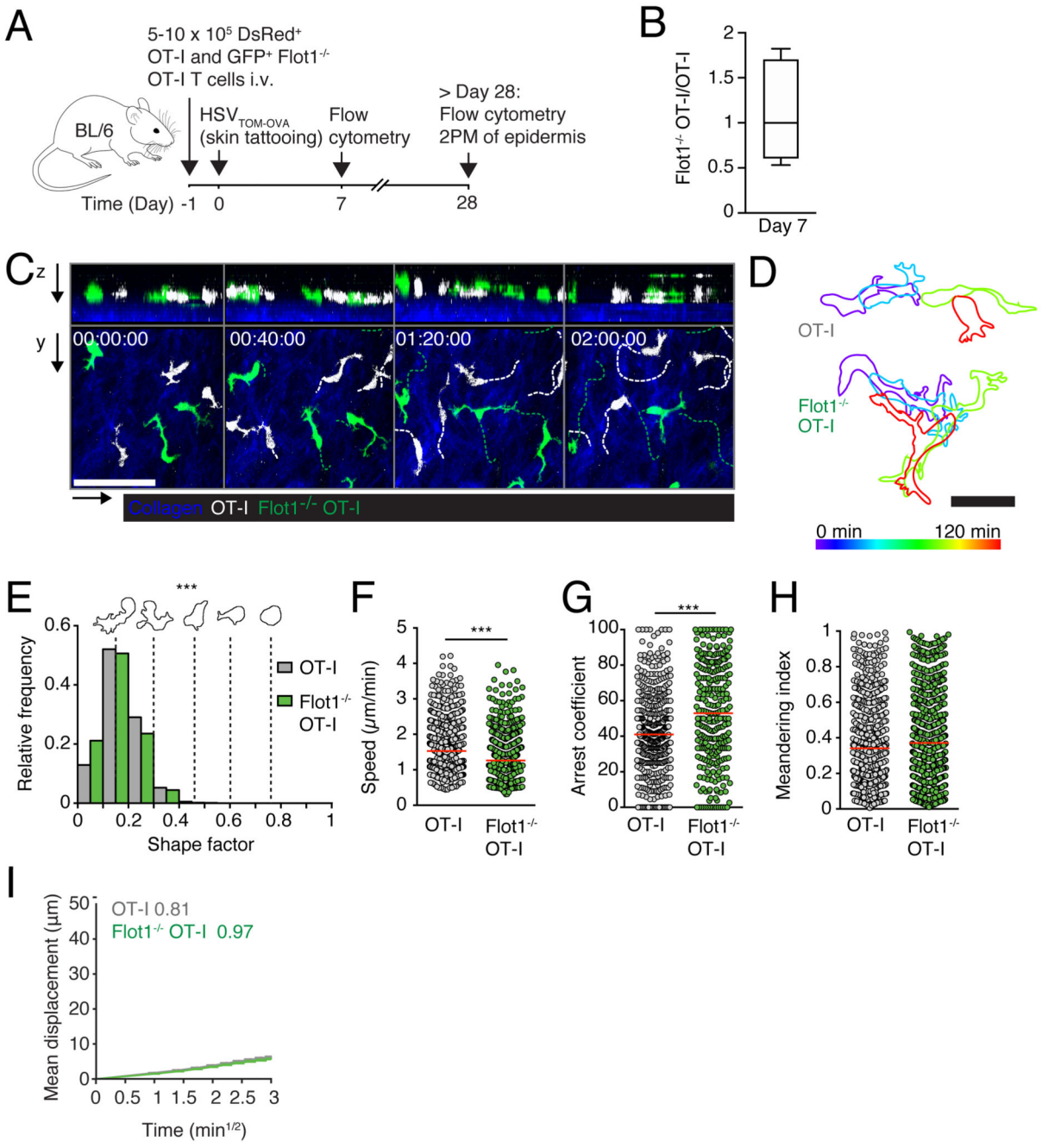

Figure 5. Epidermal Flot1$^{-/-}$ CD8^{+} T_{RM} migration.

A. Experimental layout for the generation of epidermal T_{RM} with $HSV_{TOM-OVA}$ infection. **B.** Ratio of OT-I and Flot1$^{-/-}$ OT-I T cells recovered at day 7 from $HSV_{TOM-OVA}$ infected skin. **C.** 2PM image sequence of memory OT-I and Flot1$^{-/-}$ OT-I T cells showing both xy and xz views of epidermis over 2 h of continuous imaging. OT-I cells and cell tracks in white, and Flot1$^{-/-}$ OT-I cells and tracks in green. Dermal collagen visualized by second harmonic generation shown in blue. Scale bar 50 μm; Time in h:min:s. **D.** Representative time-coded outlines of migrating memory OT-I and Flot1$^{-/-}$ OT-I T cells in the epidermis. Scale bar, 20

Europe PMC Funders Author Manuscripts

Europe PMC Funders Author Manuscripts

μm. **E.** Shape factor of epidermal OT-I and Flot1$^{-/-}$ OT-I T cells. Pooled from one experiment with n = 2 (OT-I) or n = 3 (Flot1$^{-/-}$ OT-I) mice. **F-H.** Speed (F), arrest coefficient (G) and meandering index (H) of epidermal OT-I or Flot1$^{-/-}$ OT-I T cells. Red lines depict median, each dot represents the average value for an individual track. **I.** Mean displacement versus time for datasets in E-G. Numbers indicate motility coefficient in μm^2/min. Data in B are pooled from 2 independent experiments (n = 5) and data E to I were pooled from 3 independent experiments (n = 10). Data in F were analyzed using unpaired Student's t-test, data in E, G and H using Mann-Whitney test. ***, $p < 0.001$.

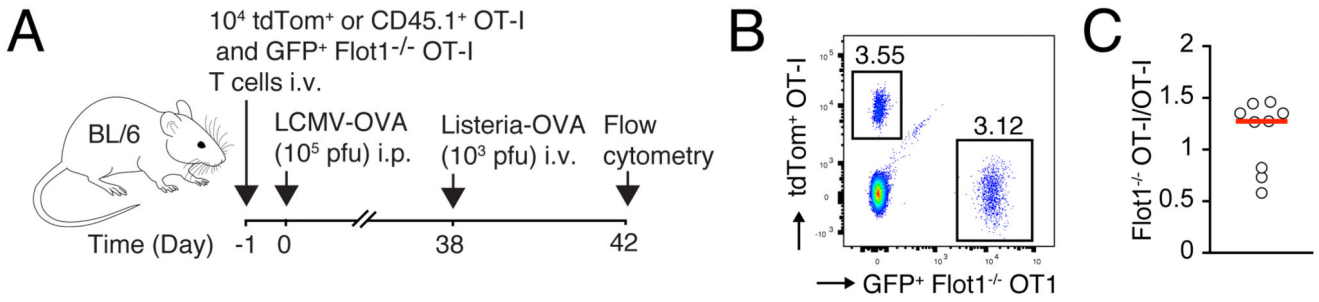

Figure 6. Secondary expansion of WT and Flot1$^{-/-}$ memory CD8^{+} T cells after rechallenge.

A. Experimental layout. **B.** Flow cytometry plot of OT-I and Flot1$^{-/-}$ OT-I T cells at day 4 post Listeria-OVA challenge. **C.** Ratio of OT-I and Flot1$^{-/-}$ OT-I T cells in spleen after normalization to pre-challenge ratio. Data in C are pooled from 2 independent experiments with a total of 9 mice.

Europe PMC Funders Author Manuscripts